Publishing House
AKAPIT

COMPUTER METHODS IN MATERIALS SCIENCE

Informatyka w Technologii Materiałów

Vol. 14, 2014, No. 2

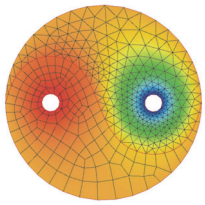

DETERMINATION OF THE FLOW STRESS MODEL OF AZ80 Mg ALLOY

TOKO TOKUNAGA[1]*, ROMAN KUZIAK[2], KIYOTAKA MATSUURA[3]

[1] Research Fellow of Japan Society for the Promotion of Science, PhD student, Graduate School of Engineering, Hokkaido University, Sapporo, Hokkaido 060-8628, Japan
[2] Institute for Ferrous Metallurgy, Gliwice, Poland
[3] Faculty of Engineering, Hokkaido University, Sapporo, Hokkaido 060-8628, Japan
**Corresponding author: ue145460@frontier.hokudai.ac.jp*

Abstract

The flow stress model of AZ80 Mg alloy, whose grain size is approximately 30 μm, is created by interpreting the experimental results with the inverse analysis. Compression tests were conducted at temperatures of 523, 573 and 623 K and at strain rates of 0.01, 0.1 and 1 s^{-1}. On the basis of the test results, the flow stress model of the Mg alloy was determined. As candidates of the flow stress model, three equations were selected and the coefficients in those equations were determined by using the inverse analysis and optimization process. In the optimization process, the measured and calculated loads were compared and the difference between them was minimized as objective functions. Consequently, the flow stress equation was chosen and the coefficients were determined. Reasonably good agreements of measured and calculated results were obtained with the equation which can be taken into account not only the softening but also the saturation of the flow stress due to the dynamic recrystallization.

Key words: computer simulation, inverse analysis, plastic deformation

1. INTRODUCTION

Mg alloys have the lowest density among all conventional structural metal materials and they are characterized by a very high specific strength. Notably, among all Mg alloys, Mg-Al-Zn alloys (AZ alloys) are one of the most widely-used materials and especially AZ80 Mg alloy is known to have an attractive balance of strength, plasticity and toughness (Zhou et al., 2010). On the other hand, Mg is extremely chemically active and possesses a very high reactivity, and the wide and practical usage of Mg alloys has been limited (Ambat et al., 2000). In order to improve the corrosion resistance of Mg alloys, a number of processes have been proposed. However, problems still remain to be solved e.g. difficult surface treatment prior to the process, non-uniformity of the coating and negative effect on the environment (Gray et al., 2002). Therefore, better and promising processes have been expected, which can improve the corrosion resistance of Mg alloy. To break through this current status, the present authors developed a new process of coating Mg alloys with a thick Al layer by a conventional hot extrusion method using a convex die (Tokunaga et al., 2012). The process enables us to obtain Mg alloy bars and plates covered with Al layer and they exhibit the excellent corrosion resistance of Al. It is expected that this new coating process can provide the application of Mg alloys in a broad range of areas. However, a huge number of trial and error will be inevitable to design and optimize the process parameters for the application of this process to individual cases with different materials properties and extrusion conditions. Thus, numerical simulation can be used

 ISSN 1641-8581

as a cost-effective way in both aspects of time and energy. To implement simulations, accurate flow stress model of the material is indispensable. The flow stress model for AZ80 Mg alloy has been studied and some models were proposed (Qua et al., 2011; Quan et al., 2013; Zheng et al., 2010; Zhou et al., 2010). However, in those works, the models were directly obtained from the mechanical test, therefore, the models may be affected by the experimental errors such as effects of friction and inhomogeneities of strain, stress and temperature. Thus, in the present study, the flow stress model of AZ80 Mg alloy was developed with inverse analysis, which is capable of describing real properties of materials, independently of the disturbances affecting the tests (Szeliga et al., 2006).

Additionally, the above works were conducted only with as-cast alloys whose grain diameter is over 100 μm, which is very coarse for Mg alloys. Mg alloys are known to have very low formability at room temperature with the hexagonal close-packed crystal structure and because of the drawback, they are often required to have fine grains (Kang et al., 2007). Therefore, the AZ80 Mg alloy with finer grain size is chosen for the model in the present study.

2. EXPERIMENT

2.1. Material and test conditions

In the present study, to get the plasticity properties of the AZ80 Mg alloy, a compression test was conducted, because it is the simplest method.

A commercially extruded bar of a Mg-8.2 mass% Al-0.56 mass% Zn-0.44 mass% Mn alloy with a diameter of 42 mm was extruded into a rod having a diameter of 12 mm, and then it was mechanically machined to make specimens of 8 mm diameter and 10 mm height. The specimens were solution–treated at 673 K for 5 h, and then precipitation-treated again at 623 K for 1 h. The grain size of the Mg alloy after those treatments was 28 μm.

The constant strain rate tests were performed with the Gleeble 3800 simulator at temperatures of 523, 573 and 623 K and at strain rates of 0.01, 0.1 and 1 s^{-1}. The ram speed was constantly adjusted during the compression tests to obtain the constant strain rates. Two specimens were used for each condition of the tests in order to confirm the repeatability. The compression direction corresponds to the extrusion direction. Temperature was measured with a thermocouple spot-welded to the side surface of the specimens at centre of the height.

2.2. Results

Figure 1 shows the load-displacement curves obtained from the compression tests. From the figures, it can be seen that the flow stress decreases as the compression-test temperature increases, but increases as the strain rate increases. Figure 2 shows the temperature changes monitored during the tests.

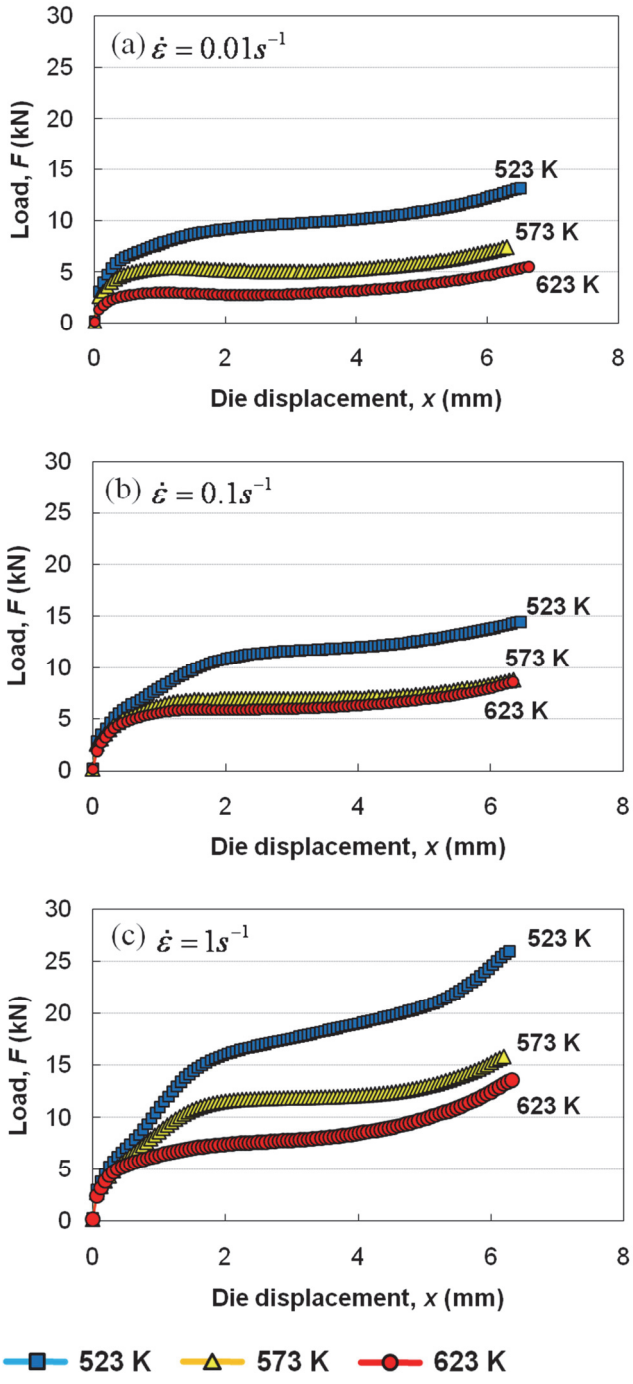

Fig. 1. Loads measured in the uniaxial compression test of AZ80 Mg alloy at a strain rate of (a) 0.01 s^{-1}, (b) 0.1 s^{-1} and (c) 1 s^{-1}.

From the figure, it can be said that reasonably stable temperatures were maintained in the tests at lower strain rates (0.01 and 0.1 s^{-1}). On the other hand, in the tests at higher strain rate (1 s^{-1}), a significant temperature drops were observed at the last stage of the tests. This temperature change is due to the heat generation by deformation, heat transfer to the environment and automated control by the Gleeble 3800 simulator.

This research was undertaken as a result of a concern that the direct interpretation of the material data from the plasticity test may result in inaccurate flow stress models due to the inhomogeneities of temperatures and stress and strain fields. Therefore, in order to minimize the influence of those inhomogeneities, inverse analysis was applied. The inverse analysis allows us to obtain values of the material parameters independently of the inhomogeneities occurring in the plasticity tests (Szeliga et al., 2006).

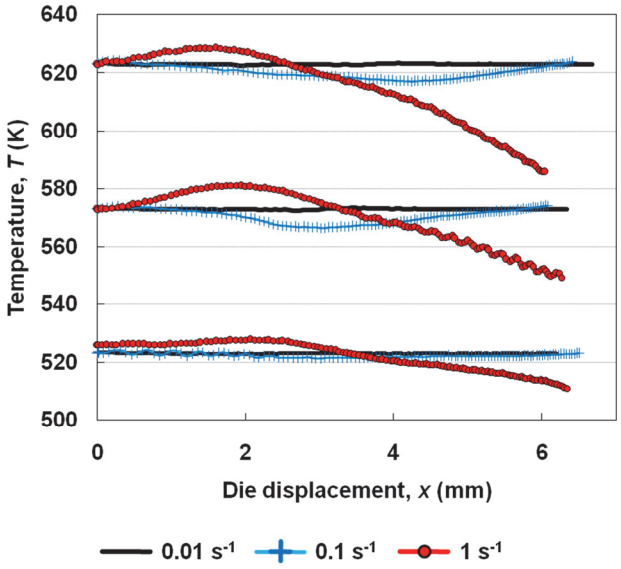

Fig. 2. Temperatures monitored during the tests.

3. INVERSE ANALYSIS

The inverse analysis was performed in the present study with the two-step algorithm (Szeliga et al., 2006) consisting of "Preliminary inverse approach" (Step 1) and "Identification" (Step 2). Since detailed explanation of the two-step algorithm can be found elsewhere (Szeliga et al., 2006), only the brief explanation is given below.

3.1. Preliminary inverse approach (Step 1)

3.1.1. Methodology

In Step 1, stress-strain curves were obtained by searching for the minimum of the following objective function:

$$\Phi_1 = \sqrt{\frac{1}{N_t}\sum_{i=1}^{N_t}\left[\frac{1}{N_s}\sum_{j=1}^{N_s}\left(\frac{F_{ij}^m - F_{ij}^c}{F_{ij}^m}\right)^2\right]} \qquad (1)$$

where N_t is number of tests, N_s is number of load measurement sampling points in one test and F^m and F^c are measured and calculated loads, respectively. The measured temperatures shown in figure 2 were used as a boundary condition of calculations in both Step 1 and Step 2 of the inverse analysis.

3.1.2. Results

The stress-strain curves obtained as the results of Step 1 are shown in figure 3. The curves were obtained from the load-displacement curves based on the experimental data and the effect of disturbances such as inhomogeneities of strain, stress and temperature is taken into account. Therefore, the curves show the material parameters independently of the inhomogeneities.

However, those curves show the material properties only under the conditions where the compression tests were conducted and to perform simulations, flow stress models should be fit in wide ranges of temperature and strain rate continuously. Therefore, in order to obtain a model, which can be applied under the wide range of conditions, the flow stress model is developed in Step 2 of the inverse analysis. In following sections, three equations are selected as candidates of the flow stress model and the most appropriate model is determined.

3.2. Identification (Step 2)

3.2.1. Methodology

As mentioned in the previous section, three flow stress models are selected as candidates and those equations are introduced in this section.

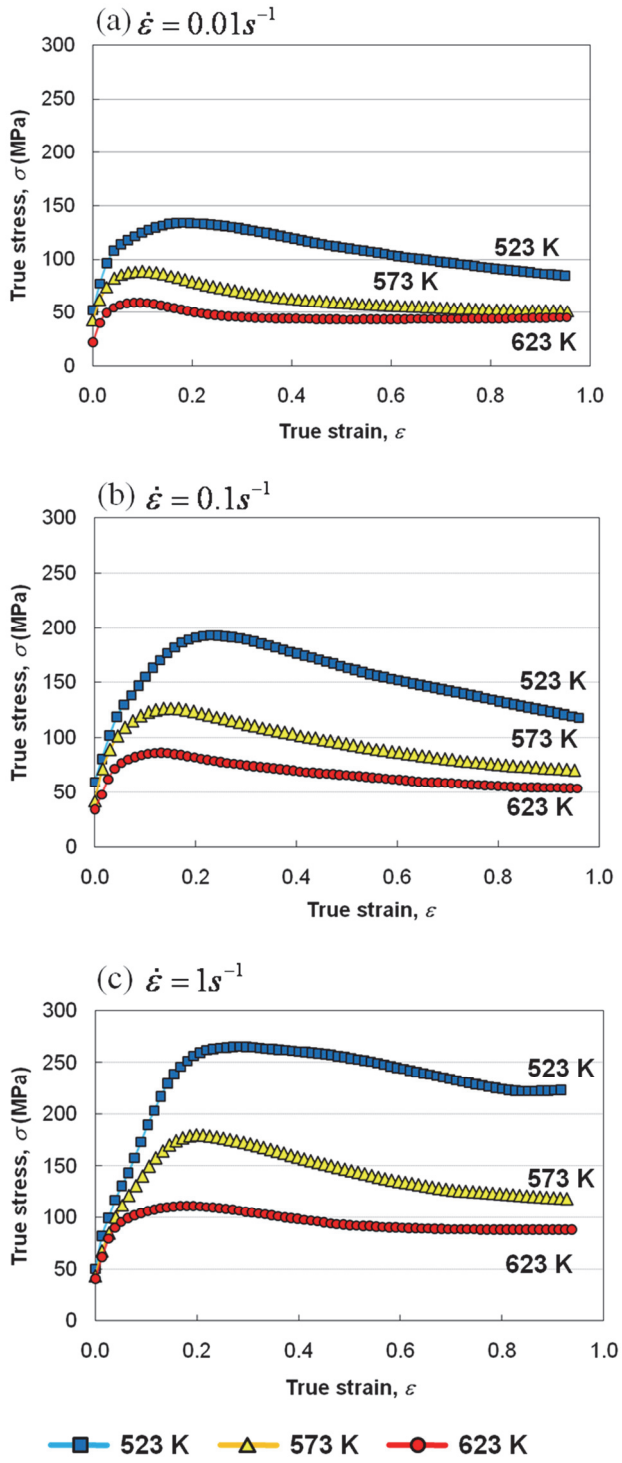

Fig. 3. Stress-strain curves determined in Step 1 of the inverse analysis at a strain rate of (a) 0.01 s^{-1}, (b) 0.1 s^{-1} and (c) 1 s^{-1}.

It is known that Mg alloys are prone to have dynamic recrystallization (DRX) during hot deformation (Zhou et al., 2010). Therefore, it is necessary to consider the influence of DRX, which causes softening of the material. The tendency of DRX depends on process conditions and is described by the Zener-Hollomon parameter (Bhattacharya & Wynne, 2012):

$$Z = \dot{\varepsilon} exp\left(\frac{Q_{def}}{RT}\right) \quad (2)$$

where $\dot{\varepsilon}$ is strain rate, Q_{def} is activation energy for deformation, R is gas constant and T is temperature. The higher the Z value, the higher tendency of DRX exists.

One of the attempts to describe flow stresses in a hot forming process taking into account DRX is Hansel and Spittel equation (Mehtedi et al., 2014, Tang et al., 2013):

$$\sigma_p = g_1 \varepsilon^{g_2} \dot{\varepsilon}^{g_3} exp\{-g_4(T-273)\} exp(-g_5\varepsilon) \quad (3)$$

where ε is strain, g_1, g_2, g_3, g_4 and g_5 are coefficients.

This model is one of the most well-known models which can describe both hardening and softening effects. However, due to its strong softening effect, flow stress calculated from this equation can converge to zero as the strain takes larger value (Mehtedi et al., 2014; Tang et al., 2013). This is inappropriate and is the main drawback of this model. In the case of real materials, the flow stress gradually decreases due to DRX, reaches saturation and consequently remains constant (Sellars, 1979). Therefore, the flow stress model which can consider both the softening and saturation was also considered with following equation (Gavrus et al., 1996):

$$\sigma_p = \sqrt{3}\left[W h_1 \varepsilon^{h_2} exp\left(\frac{-h_4}{T}\right) + (1-W) h_5 exp\left(\frac{h_6}{T}\right)\right]\left(\sqrt{3}\dot{\varepsilon}\right)^{h_3} \quad (4)$$

where $W = exp(-h_7\varepsilon)$, h_1, h_2, h_3, h_4, h_5, h_6 and h_7 are coefficients.

The terms multiplied by W and $(1-W)$ indicate the hardening and softening, respectively. As is clear from the equation, the contribution of softening term increases when the strain increases.

The following equation (Davenport et al., 1999; Kowalski et al., 2000) was selected as the most advanced model in this study:

$$\sigma_p = \sigma_0 + \left(\sigma_{ss(e)} - \sigma_0\right)\left[1 - exp\left(-\frac{\varepsilon}{\varepsilon_r}\right)\right]^{\frac{1}{2}} - R \quad (5)$$

where

$$R = \begin{cases} 0 & \varepsilon \le \varepsilon_c \\ \left(\sigma_{ss(e)} - \sigma_{ss}\right)\left[1 - exp\left(-\left[\frac{\varepsilon - \varepsilon_c}{\varepsilon_{xr} - \varepsilon_c}\right]^2\right)\right] & \varepsilon > \varepsilon_c \end{cases}$$

$$\sigma_0 = \frac{1}{\alpha_0}\sinh^{-1}\left(\frac{Z}{A_0}\right)^{\frac{1}{n_0}}, \quad \sigma_{ss} = \frac{1}{\alpha_{ss}}\sinh^{-1}\left(\frac{Z}{A_{ss}}\right)^{\frac{1}{n_{ss}}},$$

$$\sigma_{ss(e)} = \frac{1}{\alpha_{sse}}\sinh^{-1}\left(\frac{Z}{A_{sse}}\right)^{\frac{1}{n_{sse}}}$$

$$\varepsilon_r = \frac{1}{3.23}\left[q_1 + q_2\left(\sigma_{ss(e)}\right)^2\right],\ \varepsilon_{xr} - \varepsilon_c = \frac{\varepsilon_{xs}-\varepsilon_c}{1.98},$$
$$\varepsilon_c = C_c\left(\frac{Z}{\sigma^2_{ss(e)}}\right)^{N_c} \text{ and } \varepsilon_{xs} - \varepsilon_c = C_x\left(\frac{Z}{\sigma^2_{ss(e)}}\right)^{N_x}.$$

σ_0, $\sigma_{ss(e)}$, ε_r, ε_c, ε_{xr} and ε_{xs} are characteristic stress or strain which are defined in stress strain curves. A_0, A_{ss}, A_{sse}, n_0, n_{ss}, n_{sse}, α_0, α_{ss}, α_{sse}, q_1, q_2, N_c, N_x, C_c and C_x are coefficients.

Similarly to equation (4), equation (5) is capable of describing softening followed by saturation. Since it contains 16 coefficients, equation (5) is more flexible to temperature and strain rate than equation (4).

The coefficients in the equations (3), (4) and (5) were determined by using the optimization process. In the optimization process, the minimum of the following objective function, Φ_2, was searched.

$$\Phi_2 = \sqrt{\frac{1}{N_t}\sum_{i=1}^{N_t}\left[\frac{1}{N_s}\sum_{j=1}^{N_s}\left(\frac{\sigma_{ij}^1-\sigma_{ij}^c}{\sigma_{ij}^1}\right)^2\right]} \qquad (6)$$

N_t is number of tests, N_s is number of stress sampling points in one test from Step 1 and σ^l, σ^c are calculated stresses from Step 1 and calculated stresses with each equation, respectively. Detailed process of the calculation can be found elsewhere (Pietrzyk, 2000) and is not repeated here. Friction coefficient was determined as 0.12 in our preliminary investigation for the hot compression tests performed with the Gleeble 3800 simulator. In the present calculation, the coefficient was used in the friction model proposed by Chen and Kobayashi (1989):

$$\tau = m\sigma_p arctg\frac{\Delta v}{c} \qquad (7)$$

where m is friction coefficient, Δv is relative slip velocity and c is a constant. The value of c was assumed to be $1.0\cdot10^{-3}$ in the present work. We assume that the friction coefficient is not affected significantly by test temperature and strain rate based on Gontarz et al. (2011).

Equations (3), (4) and (5) were fit to the stress-strain curves obtained from Step 1 and the obtained coefficients were used as starting point for the optimization of Φ_2. This process saves the computing time significantly.

3.2.2. Results

The coefficients and objective function Φ_2 obtained from the optimization process are given in table 1. The objective function Φ_2 represents the accuracy of the model and smaller the function is, the better accuracy the model has. The coefficient Q_{def} for equation (5) indicates the activation energy in equation (2).

3.3. Validation of the model

In order to confirm the validities of the models, the forces measured in the tests and calculated by using the FE code with the selected model implemented in the constitutive law were compared. Figures 4, 5 and 6 show comparisons between experimental and calculated results in each equation (3), (4) and (5), respectively. Analysis of the results revealed that perfect accuracy was not reached for the whole ranges of strain rate and temperature with all the equations. However, a good agreement between measurements and calculations was obtained for equation (5), which showed the lowest value of the objective function Φ_2 in table 1. Also, reasonably

Table 1. *Coefficients in equations (3), (4) and (5) and the objective functions obtained from the inverse analysis.*

Equation (3)	$\Phi_2 = 0.1257$					
g_1	g_2	g_3	g_4	g_5	-	-
3724.4	0.274	0.158	0.00832	1.061	-	-
Equation (4)	$\Phi_2 = 0.1097$					
h_1	h_2	h_3	h_4	h_5	h_6	h_7
5.923	0.538	0.1592	2313.4	0.444	2820.7	5.304
Equation (5)	$\Phi_2 = 0.079$					
A_0	$n0$	$\alpha0$	A_{sse}	n_{sse}	α_{sse}	A_{ss}	n_{ss}
$0.302\cdot10^{14}$	480.6	0.0445	$0.167\cdot10^{13}$	6.344	0.0064	$0.41\cdot10^{14}$	7.622
α_{ss}	q_1	q_2	C_c	Nc	C_x	N_x	Q_{def}
0.008	0.369	1×10-10	0.0698	0.0304	0.0008	0.358	145700

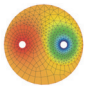

good agreement was obtained for equation (4). Therefore, it was found that equation (4) which is simpler was the most appropriate as the flow stress model of the AZ80 Mg alloy.

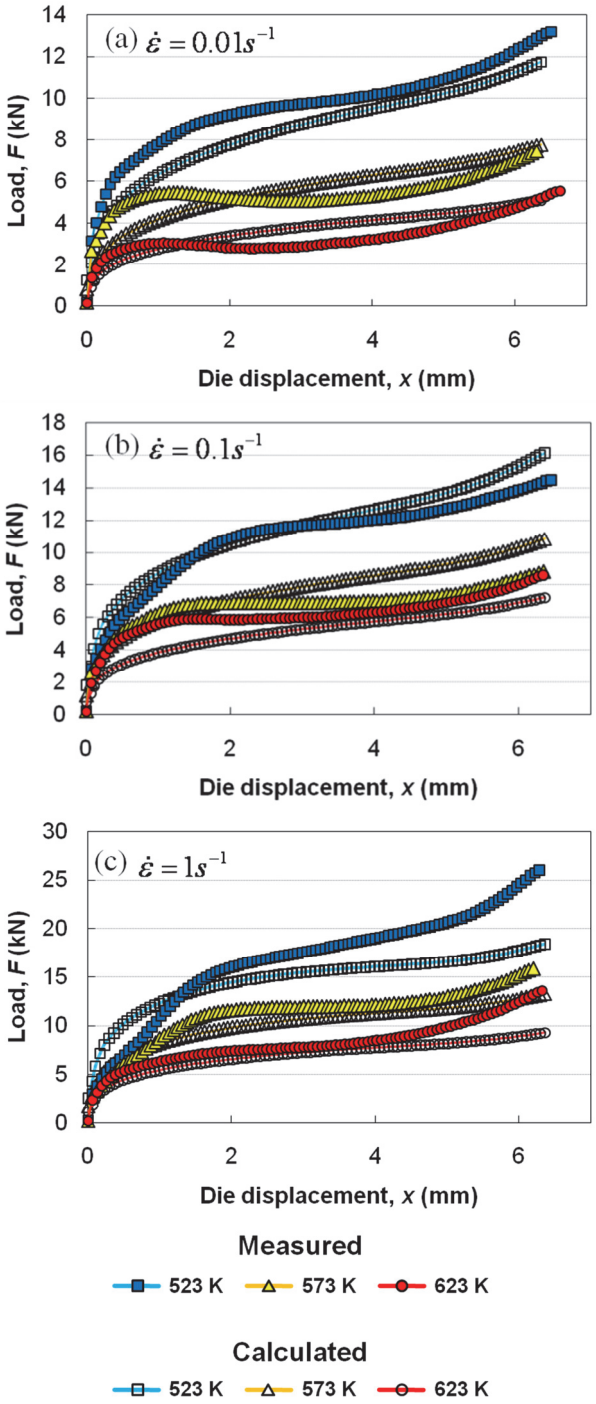

Fig. 4. Comparison of measured forces (with filled markers) with forces calculated by using the FE code with equation (3) implemented in the constitutive law (with open markers). The strain rates are (a) 0.01 s^{-1}, (b) 0.1 s^{-1} and (c) 1 s^{-1}.

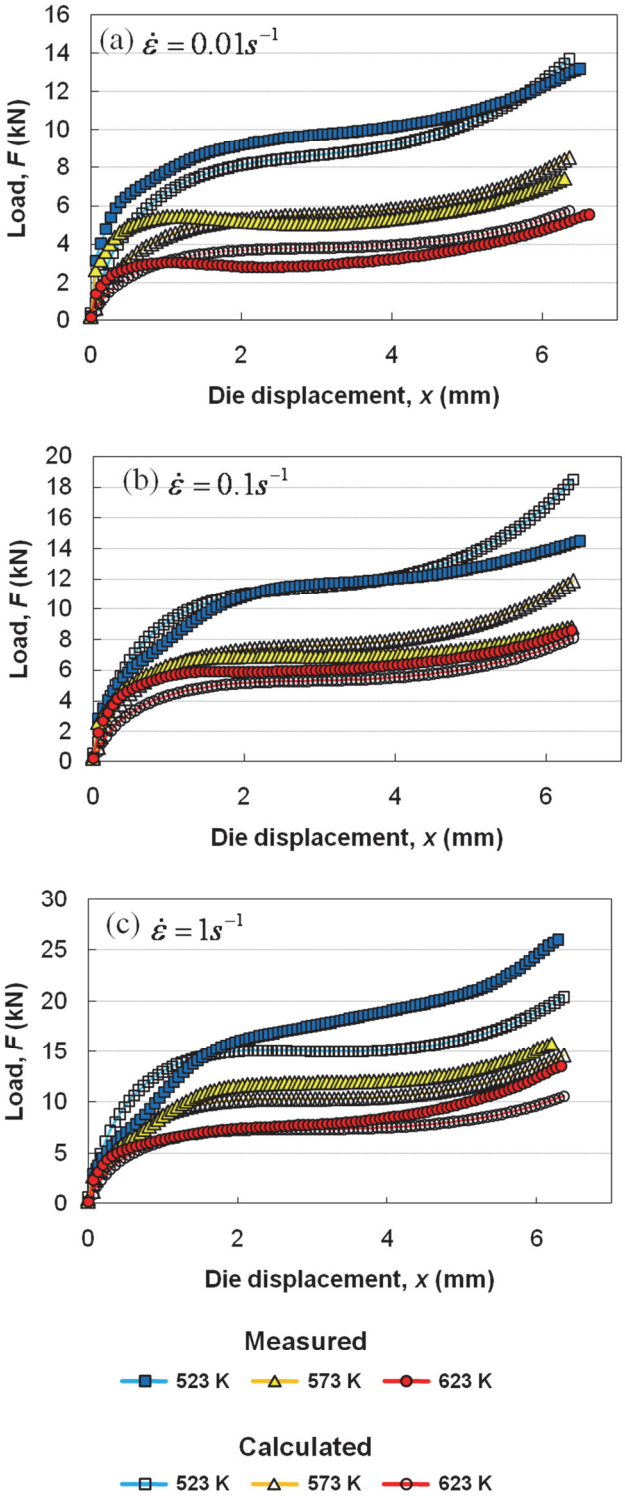

Fig. 5. Comparison of measured forces (with filled markers) with forces calculated by using the FE code with equation (4) implemented in the constitutive law (with open markers). The strain rates are (a) 0.01 s^{-1}, (b) 0.1 s^{-1} and (c) 1 s^{-1}.

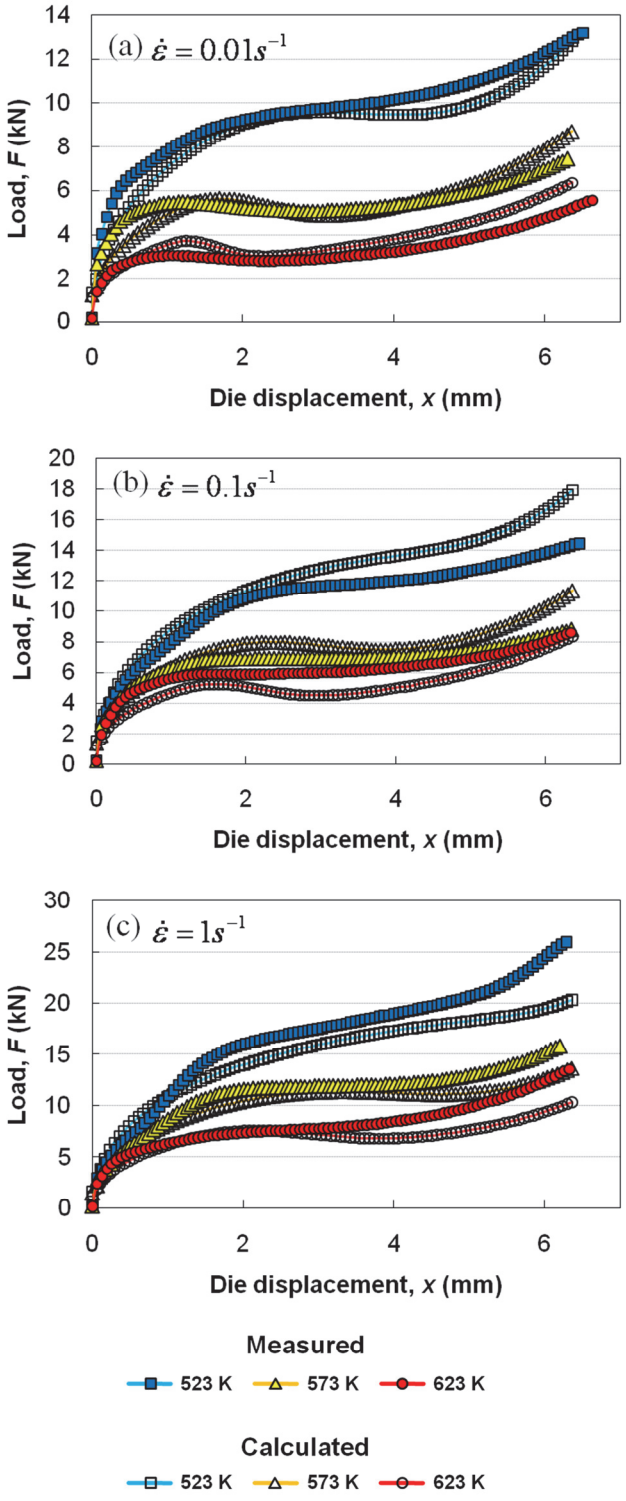

Fig. 6. Comparison of measured forces (with filled markers) with forces calculated by using the FE code with equation (5) implemented in the constitutive law (with open markers). The strain rates are (a) 0.01 s^{-1}, (b) 0.1 s^{-1} and (c) 1 s^{-1}.

4. CONCLUSIONS

Flow stress model for AZ80 Mg alloy has been developed on the basis of the inverse analysis of compression tests. The following conclusions were obtained.

1. Although perfect agreement was not obtained in the whole investigated ranges of temperature and strain rate, reasonably good agreements of measured and calculated results were obtained with equations which can take into account not only the softening but also the saturation of the flow stress due to the dynamic recrystallization.
2. The best agreement between measurements and calculations was obtained with an equation with 16 coefficients. However, a simpler equation was eventually selected as the flow stress model of AZ80 Mg alloy because it is simpler and exhibited the reasonably good accuracy.

Consequently, the flow stress model obtained for AZ80 Mg alloy in this study is:

$$\sigma_p = \sqrt{3}\left[exp(-5.304\cdot\varepsilon)\cdot 5.923\varepsilon^{0.538} \cdot exp\left(\frac{-2313.4}{T}\right) + \{1-exp(-5.304\cdot\varepsilon)\}\cdot 0.444 \cdot exp\left(\frac{2820.7}{T}\right)\right]\left(\sqrt{3}\dot{\varepsilon}\right)^{0.1592}$$

where ε is strain, T is temperature and $\dot{\varepsilon}$ is strain rate.

Acknowledgements

Financial support by JSPS KAKENHI Grant Numbers 25·1024 is gratefully acknowledged.

REFERENCES

Ambat, R., Aung, N.N., Zhou, W., 2000, Evaluation of microstructural effects on corrosion behaviour of AZ91D magnesium alloy, *Corrosion Science*, 42, 1433-1455.

Bhattacharya, R., Wynne, B.P., 2012, *Scripta Materialia*, Flow softening behavior during dynamic recrystallization in Mg–3Al–1Zn magnesium alloy, 67, 277-280.

Davenport, S.B., Silk, N.J., Sparks, C.N., Sellars, C.M., 1999, Development of constitutive equations for the modelling of hot rolling, *Materials Science and Technology*, 16, 1-8.

Gavrus A., Massoni E., Chenot J.L., 1996, An inverse analysis using a finite element model for identification of rheological parameters, *Journal of Materials Processing Technology*, 60, 447-454.

Gontarz, A., Dziubinska, A., Okon, L., 2011, Determination of Friction Coefficients at Elevated Temperatures for Some Al, Mg and Ti Alloys, *Archives of Metallurgy and Materials*, 56, 379-384.

Gray, J.E., Luan, B., 2002, Protective coatings on magnesium and its alloys – a critical review, *Journal of Alloys and Compounds*, 336, 88-113.

Kang, S.H., Lee, Y.S., Lee, J.H., 2007, Effect of grain refinement of magnesium alloy AZ31 by severe plastic defor-

mation on material characteristics, *Journal of Materials Processing Technology*, 201, 436-440.

Kobayashi, S., Oh, S.I., Altan, T., 1989, *Metal forming and the finite element method*, Oxford University Press, New York, Oxford.

Kowalski, B., Sellars, C.M., Pietrzyk, M., 2000, Development of a computer code for the interpretation of results of hot plane strain compression tests, *ISIJ International*, 40, 1230-1236.

Mehtedi, M. El., Musharavati, F., Spigarelli, S., 2014, Materials & Design, Modelling of the flow behaviour of wrought aluminium alloys at elevated temperatures by a new constitutive equation, 54, 869-873.

Pietrzyk, M., 2000, Finite element simulation of large plastic deformation, *Journal of Materials Processing Technology*, 106, 223-229.

Qua, G.Z., Shia, Y., Wang, Y.X., Kang, B.S., Ku, T.W., Song, W.J., 2011, Constitutive modeling for the dynamic recrystallization evolution of AZ80 magnesium alloy based on stress–strain data, *Materials Science and Engineering*, A528, 8051-8059.

Quan, G.Z., Shi, Y., Yu, C.T., Zhou, J., 2013, The Improved Arrhenius Model with Variable Parameters of Flow Behavior Characterizing for The As-Cast AZ80 Magnesium Alloy, *Materials Research*, 16, 785-791.

Sellars, C.M., 1979, Physical metallurgy of hot working, in: *Hot working and forming processes*, (eds), Sellars, C.M., Davies, G.J., The Metals Soc., London, 3-15.

Szeliga, D., Gawad, J., Pietrzyk, M., 2006, Inverse analysis for identification of rheological and friction models in metal forming, *Computer Methods in Applied Mechanics and Engineering*, 195, 6778-6798.

Tang, B., Yuan, Z., Cheng, G., Huang, L., Zheng, W., Xie, H., 2013, Experimental verification of tailor welded joining partners for hot stamping and analytical modeling of TWBs rheological constitutive in austenitic state, Materials Science and Engineering A, 585, 304-318.

Tokunaga, T., Matsuura, K., Ohno, M., 2012, Aluminum Coating on Magnesium-Based Alloy by Hot Extrusion and Its Characteristics, *Materials Transactions*, 53, 1034-1041.

Zheng, Q.G., Ying, T., Jie, Z., 2010, Dynamic softening behaviour of AZ80 magnesium alloy during upsetting at different temperatures and strain rates, *Proceedings of the Institution of Mechanical Engineers, Part B: Journal of Engineering Manufacture*, 224, 1707-1716.

Zhou, H.T., Li, Q.B., Zhao, Z.K., Liu, Z.C., Wen, S.F., Wang, Q.D., 2010, Hot workability characteristics of magnesium alloy AZ80—A study using processing map, *Materials Science and Engineering A*, 527, 2022-2026.

WYZNACZANIE MODELU NAPRĘŻENIA UPLASTYCZNIAJĄCEGO DLA STOPU MAGNEZU AZ80

Streszczenie

Model naprężenia dla stopu magnezu AZ80 o wielkości ziarna około 30 μm opracowano na podstawie interpretacji danych doświadczalnych za pomocą rozwiązania odwrotnego. Próby ściskania próbek osiowosymetrycznych przeprowadzono w temperaturach 523, 573 i 623 K z prędkościami odkształcenia 0.01, 0.1 i 1 s^{-1}. Uzyskane wyniki posłużyły do opracowania modelu. Przy budowie modelu wybrano trzy równania i współczynniki w tych równaniach wyznaczono za pomocą rozwiązania odwrotnego. W procedurze optymalizacyjnej porównywano zmierzone i obliczone siły a różnica między nimi była minimalizowana jako funkcja celu. W konsekwencji wybrano równanie najlepiej opisujące zachowanie się materiału i wyznaczono współczynniki w tym równaniu. Równanie to uwzględnia zarówno umocnienie materiału jak i mięknięcie w wyniku dynamicznej rekrystalizacji oraz stan ustalony przy większych odkształceniach. Uzyskano dobrą zgodność między obliczonymi i zmierzonymi siłami w próbie ściskania.

Received: May 11, 2014
Received in a revised form: July 7, 2014
Accepted: July 15, 2014